Arabian Journal of Chemistry (2020) **13**, 227–241

King Saud University

Arabian Journal of Chemistry

www.ksu.edu.sa
www.sciencedirect.com

ORIGINAL ARTICLE

Core-shell zirconia-coated magnetic nanoparticles offering a strong option to prepare a novel and magnetized heteropolyacid based heterogeneous nanocatalyst for three- and four-component reactions

Somayeh Zolfagharinia, Eskandar Kolvari *, Nadiya Koukabi, Maliheh M. Hosseini

Department of Chemistry, Semnan University, Semnan, Iran

Received 28 December 2016; accepted 1 April 2017
Available online 10 April 2017

KEYWORDS

Nano-Fe_3O_4@ZrO_2 supported PMA;
Core-shell zirconia-coated magnetite nanoparticles;
Heterogeneous nanocatalyst;
Reusability;
Multicomponent reaction (MRCs)

Abstract A new type of magnetically-separable nanocatalyst was prepared through the immobilization of phosphomolybdic acid ($H_3PMo_{12}O_{40}$) in 10–30 wt.% on the surface of core-shell zirconia-coated magnetite nanoparticle (nano-Fe_3O_4@ZrO_2). The developed heterogeneous nano-sized acid catalyst named nano-Fe_3O_4@ZrO_2 supported PMA (or n-Fe_3O_4@ZrO_2/PMA) was characterized using several techniques such as FT-IR, XRD, FE-SEM, VSM, EDX, TEM and TGA. The characterization data derived from FT-IR spectroscopy exhibited that $H_3PMo_{12}O_{40}$ species on the support retained their Keggin structures. Additionally, the potentiometric titration with *n*-butylamine was employed to measure the acidity content of the as-obtained catalyst. Surprisingly, this novel active solid acid catalyst displayed to have a higher number of surface active sites compared to its homogeneous analogues. Besides, the catalytic activity of the catalyst was evaluated in multicomponent reactions (MRCs) for the rapid and efficient one-pot synthesis of 2, 4, 5-trisubstituted and 1, 2, 4, 5-tetrasubstituted imidazoles in high yields and selectivity. The sample of 20 wt.% displayed higher acidity content which led to its enhanced activity in the catalytic transformation. Moreover, the catalyst could be easily reused without deactivation after five runs, which made it a promising catalyst for practical and large-scale applications. This outstanding reusability was ascribed to the strong attachment of PMA molecules on the n-Fe_3O_4@ZrO_2 support material.

* Corresponding author. Fax: +98 23 336 54110.
E-mail address: kolvari@semnan.ac.ir (E. Kolvari).
Peer review under responsibility of King Saud University.

Production and hosting by Elsevier

1. Introduction

From the initiation of the recent century, chemists' interests for the development of simple and safe economic and environmental routes in the field of synthetic organic chemistry have been increased. As a result, research focuses have grown into "Green Chemistry". The green

http://dx.doi.org/10.1016/j.arabjc.2017.04.004
1878-5352

chemistry principles explore every avenue in the research for new methodologies in which significant reduction in by-products, wastes, and energy costs is emerged (Cave et al., 2001). One particular area, through which the green chemistry goals can be achieved, involves replacing corrosive and toxic liquid acids such as HF and H_2SO_4 in the catalyst systems with environmental friendly heterogeneous solid acids (Corma and Martínez, 1993; Misono and Okuhara, 1993; Thomas, 1992). To date, myriad examples of solid acid catalysts such as clays, zeolites, sulfated metal oxides or carbons and heteropolyacids have attracted immense attention of researchers (Clark, 2002; Mitsutani, 2002; Sheldon and Downing, 1999; Wang et al., 2010). On account of being unique in strong BrØnsted acidity, lower corrosivity and higher catalytic activity, heteropolyacid compounds, among others, have been applied in several large-scale industrial processes (Kim et al., 2006; Kozhevnikov, 1998; Long et al., 2010). However, in the bulk form, heteropolyacids possess very low surface area and high solubility in polar medium leading to limitation in the exertion of potentially catalytic performance and difficulties in catalyst recovery (Damyanova et al., 1999). In order to overcome these shortcomings, researchers have endeavored so as to improve the catalytic efficacy and stability of heteropolyacids by the help of varied methods such as pillaring layered clays with polyanions, dispersing heteropolyacids on solid supports with high surface area, changing countercations in heteropolyacids, immobilizing heteropolyacids into an organic polymer and preparing nanoscale polyoxometalate particles (Izumi et al., 1993; Long et al., 2010; Mizuno et al., 2011; Okuhara, 2003). However, in the case of applying those potentially promising reactions in practice, complete recovery will be required in the amount of those rather expensive polyoxometalate catalysts.

During the past century, with growing of nanoscience and nanotechnology, research focuses of interests have been shifted to the employment of nanometer-sized particles for the construction of a magnetically retrievable nanocatalyst system (Lim and Lee, 2010; Shylesh et al., 2010). In order that, the magnetite nanoparticles are often used to immobilize or attach non-magnetic catalytic active phases, such as metal complexes, metal or oxide nanoparticles, enzymes, or organocatalysts (Rossi et al., 2014). As a consequent, during the absence of the magnetic field, magnetic nanocatalysts can be well dispersed in the reaction mixtures, whereby a large surface area, which can be readily approached by substrate molecules, is provided. The attractive point is that, in this condition, these catalysts can be rapidly separated from the reaction mixtures through applying a permanent magnet externally when the reactions ended (Shylesh et al., 2010). These features make magnetic nanoparticles attractive candidates in the development of a cost-effective catalysis process. Possessing a large fraction of their atoms on the external surface, pristine magnetic nanoparticles will aggregate rapidly into large clusters and then will lose their unique properties related to the presence of single domains (i.e. they loss their active reaction sites and specific surface areas and therefore enhance deactivation). Addressing this thorny issue, the magnetic nanoparticles have to be stabilized through covering with appropriate coating agents such as organic materials (polymers (Narayanan and El-Sayed, 2003), surfactants (Mévellec et al., 2004), dendrimers (Wu et al., 2006), and ionic liquids (Caló et al., 2003)) and inorganic compounds (silica (Pujari et al., 2014), gold (Chen et al., 2003), carbon (Chen et al., 2013), and titanium dioxide (Xuan et al., 2008)). Zirconia (ZrO_2), an inorganic coating material, is an important n-type semiconductor material with which a huge numbers of catalysis in oxidation and reduction can be operated (Kašpar et al., 2003). A closer look at ZrO_2 reveals that it exhibits attractive properties by itself, showing mild acid catalytic behavior and good chemical, mechanical and thermal stabilities (Sunita et al., 2008). Additionally, the surface hydroxyl groups of ZrO_2 possess the ability to experience a chemical interaction or strong reaction with different reagents or materials. Thus, the inclusion of Fe_3O_4 nanoparticles into a layer of ZrO_2 (Li et al., 2007), providing a core-shell structure (i.e. Fe_3O_4@ZrO_2) can raise an opportunity for the protection of Fe_3O_4 core from the irreversible coagulation or easy oxidation upon the exposure to air, and, in return, Fe_3O_4 core endows its wealthy magnetic properties. It can be concluded that the immobilization of the heteropolyacids in such a magnetically retrievable nanoparticles matrix will offer easy treatment in the production process and open up an opportunity for their applications in the chemical or pharmaceutical industry. Unfortunately, the design and development of the stable magnetic solid acid catalysts in harsh catalytic conditions are often a big challenge for catalytic chemists and are, to date, significantly less advanced than the research in other solid acid catalysts (Feyen et al., 2010; Gill et al., 2007).

As a part of our program aiming at developing heterogeneous catalysts and modification of different support materials (Hosseini et al., 2016; Kolvari et al., 2014; Kolvari et al., 2015a,b; Kolvari et al., 2016; Kolvari and Zolfagharinia, 2016; Koukabi et al., 2011, 2012), in this work, we aim to report the construction of a magnetically recoverable solid acid nanocatalyst, in which heteropolyacid molecules are immobilized on the surface of Fe_3O_4@ZrO_2 nanoparticles as there were no paper reports about their preparation and applications. Preparation of Fe_3O_4@ZrO_2 nanoparticles was performed through a simple sonication since the reactions of Fe_3O_4 core and ZrO_2 shell are facile and rapid. Subsequently, we hypothesized that the high surface area of Fe_3O_4@ZrO_2 nanoparticles and the high reactivity of their surface hydroxyl groups can be simultaneously employed so as to attach heteropolyacids to them. Among the heteropolyacids, phosphomolybdic acid is one of the least expensive commercially available solid acid catalysts. Hence, it is used in many organic transformations, such as dehydration, esterification, acylation, and oxidation (Mallik et al., 2006). On the other hand, there have been no reports on the preparation of phosphomolybdic acid ($H_3PMO_{12}O_{40}$) supported on nano-Fe_3O_4@ZrO_2 and using it as a catalyst for the synthesis of biological, therapeutical and agricultural useful multisubstituted imidazoles (Antolini et al., 1999; Bossche et al., 1983; Deprez et al., 2002; Freedman and Loscalzo, 2009; Gallagher et al., 1995; Lange et al., 2005; Laszlo et al., 1999; Sarshar et al., 2000; Wang et al., 2002). Such a magnetically acid nanocatalyst displayed extraordinary catalytic performance in the multicomponent reaction for the one-pot synthesis of 2, 4, 5-trisubstituted imidazoles from the reaction of aromatic aldehydes, benzil and NH_4OAc as well as for the preparation of 1, 2, 4, 5-tetrasubstituted imidazoles from the condensation of aromatic aldehydes, amines, benzil, and NH_4OAc under solvent-free conditions. Our synthesized catalyst namely n-Fe_3O_4@ZrO_2/PMA can be readily recovered and reused with no significant loss of catalytic activity due to the efficient anchoring of heteropolyacid molecules and rapidly magnetic separation properties. In the next step, the as-synthesized catalyst was characterized *via* XRD, FE-SEM, TEM, VSM, FT-IR, EDX analyses and investigated in detail. Besides, the novel nano-Fe_3O_4@ZrO_2 supported phosphomolybdic acid possesses the advantages of being thermally stable, non-toxic, and fast-/easy-manufacturing.

2. Result and discussion

The novel n-Fe_3O_4@ZrO_2/PMA catalyst preparation was shown in Scheme 1. At first step, Fe_3O_4 nanoparticles were provided through a partial reduction coprecipitation route illustrated in the previous report (Qu et al., 1999; Sun et al., 2004b). For the preparation of Fe_3O_4@C magnetic nanoparticles a hydrothermal reaction between glucose and Fe_3O_4 magnetic nanoparticles was occurred based on the procedure previously reported (Li et al., 2007). At next step, the core-shell structured Fe_3O_4@ZrO_2 nanoparticles were synthesized by the help of a sonochemical pathway. At the last step, the Fe_3O_4@ZrO_2/PMA MNPs with varied loading amounts of PMA ranging from 10 to 30 wt.% were prepared through the immobilizing of phosphomolybdic acid on the n-Fe_3O_4@ZrO_2 support surfaces. According to the obtained

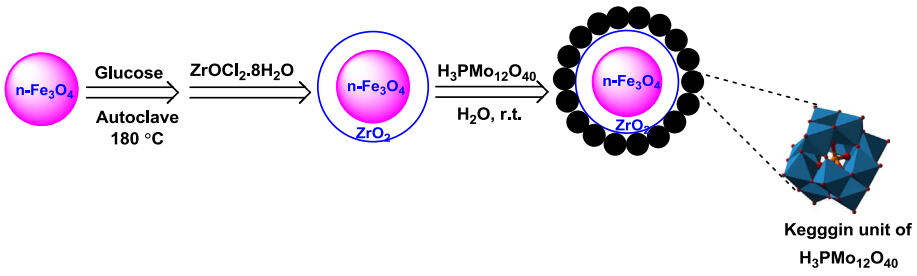

Scheme 1 Preparation of n-Fe_3O_4@ZrO_2 supported phosphomolybdic acid.

results, n-Fe_3O_4@ZrO_2/PMA 20 wt.% exhibited superior performance compared to the other PMA loaded catalysts prepared. To get additional insight into the structural features, the as-synthesized novel catalyst was fully characterized by potentiometric titration, XRD, FT-IR, TGA, FE-SEM, VSM, TEM and EDX techniques.

For the purpose of determination of the acid capacity of the synthesized catalysts with potentiometric titration, firstly, the samples of n-Fe_3O_4@ZrO_2, PMA and n-Fe_3O_4@ZrO_2/PMA (10–30 wt.%) (0.05 g) were dispersed in acetonitrile (90 ml) and allowed to be sonicated for 30 min. Then, the prepared suspension was titrated with a 0.05 mol L^{-1} solution of *n*-butylamine in acetonitrile.

3. Characterization of n-Fe_3O_4@ZrO_2/PMA

3.1. Acid-base titration

The acidity of the prepared catalysts was measured using the potentiometric titration. Based on this method, the acid capacity of the samples is mainly determined by the acidic environment around the electrode membrane. The measured electrode potential is an indicator of the acidic properties of the dispersed solid particles. An aliphatic amine, such as *n*-butylamine, with a basic dissociation constant of approximately 10^{-6}, allows the potentiometric titration of strong acids. The titration curves obtained for PMA and

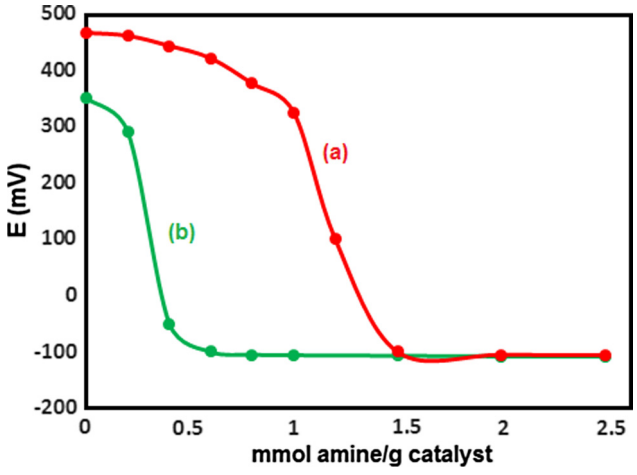

Figure 1 Potentiometric titration curves of (a) PMA and (b) n-Fe_3O_4@ZrO_2.

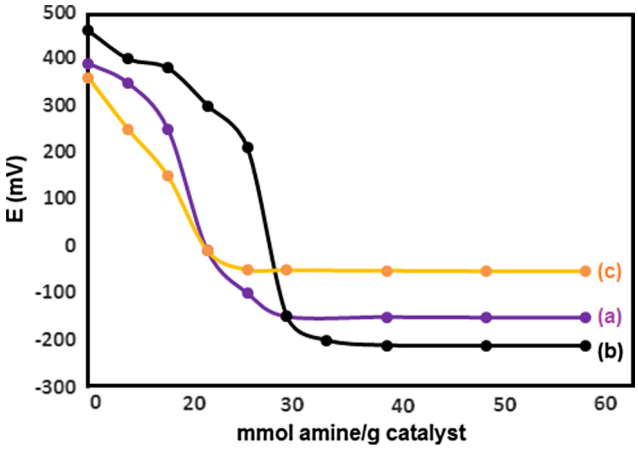

Figure 2 Potentiometric titration curves of (a) n-Fe_3O_4@ZrO_2/PMA 10 wt.%, (b) 20 wt.%, and (c) 30 wt.%.

n-Fe_3O_4@ZrO_2 are displayed in Fig. 1. It is considered that the initial electrode potential (*Ei*) indicates the maximum strength of the acid sites and that the value from which the plateau is reached (mmol amine per g catalyst) indicates the total number of acid sites that are present in the titrated solid. The acidic strength of the acid sites can be classified according to the following ranges: $Ei > 100$ mV (very strong acid sites), $0 < Ei < 100$ mV (strong acid sites), $-100 < Ei < 0$ mV (weak acid sites) and $Ei < -100$ mV (very weak acid sites) (Rafiee et al., 2008). According to the potentiometric titration curves (Fig. 1), both n-Fe_3O_4@ZrO_2 and PMA samples presented very strong acid sites ($Ei = 350$ and 466 mV, respectively). Fig. 2 exhibits the potentiometric titration results for 10–30 wt.% of the n-Fe_3O_4@ZrO_2/PMA samples that they showed the lower *Ei* values compared to the pure PMA sample. This behavior was ascribed to the textural properties of n-Fe_3O_4@ZrO_2, mainly to its surface area and its surface hydroxyl groups. In the n-Fe_3O_4@ZrO_2/PMA samples, the PMA molecule was strongly interacted with the surface hydroxyl groups of n-Fe_3O4@ZrO_2. As a result, the strength of the acid sites of PMA molecules immobilized on the surface of n-Fe_3O_4@ZrO_2 decreased. Compared to the pure PMA, the n-Fe_3O_4@ZrO_2/PMA 10 wt.% sample showed the lower *Ei* value which might be a consequence of a higher interaction of PMA molecules with the surface groups of the supports, and therefore a higher dispersion of the PMA molecules in the low concentration sample. Addition of PMA was accompanied by a gradual increase in both surface acidity and acid strength up to n-Fe_3O_4@ZrO_2/PMA 20 wt.%, and then

followed by a decrease at n-Fe_3O_4@ZrO_2/PMA 30 wt.%. These results indicated that n-Fe_3O_4@ZrO_2/PMA 20 wt.% contained the strongest acid sites (39 mmol H^+. g^{-1}). The high surface area of n-Fe_3O_4@ZrO_2 could enhance the dispersion of acidic protons up to monolayer coverage at n-Fe_3O_4@ZrO_2/PMA 20 wt.%. The further increase in PMA content above monolayer led to the aggregation of PMA on the support surface and resulted in the decrease in the surface acidity.

3.2. FT-IR analysis of the samples

For the evaluation of the successfully PMA attachment onto the surface of nano-Fe_3O_4@ZrO_2, the samples of nano-Fe_3O_4, nano-ZrO_2, PMA as well as nano-Fe_3O_4@ZrO_2/PMA were studied with FT-IR spectroscopy (Fig. 3). Compared with the FT-IR spectra of nano-Fe_3O_4 and nano-ZrO_2 spectra, nano-Fe_3O_4@ZrO_2/PMA showed the characteristic absorbance of Fe_3O_4 at 547 cm^{-1} and the strong stretching vibrations of Zr-O at 632 cm^{-1} as well (Sarkar et al., 2010). In comparison with PMA, the nano-Fe_3O_4@ZrO_2/PMA sample displayed the peaks at 1070 cm^{-1} (P-O stretching vibration), 960 cm^{-1} (MO = O_{tet} stretching vibration), 838 cm^{-1} (MO-O_c-MO stretching vibration), and 780 cm^{-1} (MO-O_e-MO stretching vibration) that confirmed the existence of PMA on the support in the Keggin structure (Rao et al., 2009). The absorbance appeared at 1637 and 3450 cm^{-1} is attributed to the presence of –OH and H–O–H groups. The results altogether confirmed the attachment of PMA on the nano-Fe_3O_4@ZrO_2 support.

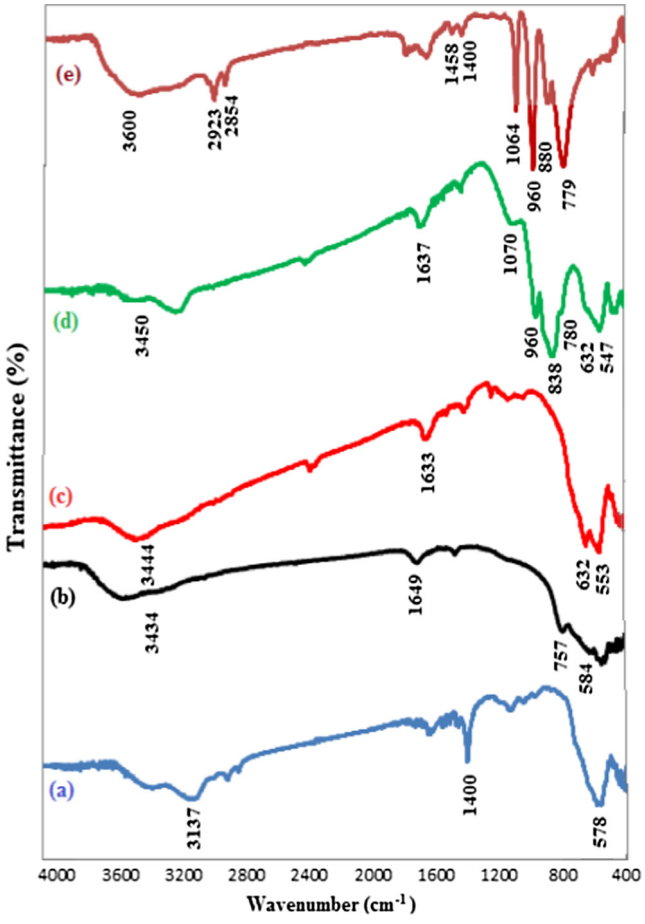

Figure 3 FT-IR spectra of (a) nano-Fe_3O_4, (b) nano-ZrO_2, (c) nano-Fe_3O_4@ZrO_2, (d) nano-Fe_3O_4@ZrO_2/PMA 20 wt.% and (e) PMA.

3.3. XRD (X-ray diffraction) analysis

X-ray diffraction was employed to analyze the purity and crystal structure of the catalyst. Fig. 4a–c represents the XRD patterns of nano-Fe_3O_4, nano-Fe_3O_4@ZrO_2 as well as nano-Fe_3O_4@ZrO_2/PMA, respectively. Cubic structure of Fe_3O_4 is confirmed by the peaks appeared at the values of 2θ equal to 30.24° (220), 35.58° (311), 43.29 ° (400), 53.7 ° (422), 57.32 ° (511) and 62.80° (440) which are in agreement with the JCPD 19-0629 standard (Fig. 2a) (Zhao et al., 2016). In the XRD of nano-Fe_3O_4@ZrO_2 sample, in addition to the Fe_3O_4 diffraction peaks, two small non-magnetic related signals located in 50.48° (112) and 60.35° (211) are detected which are matched with the standard data for ZrO_2 (JCPDS file no. 88-1007) (Kumar et al., 2013). Besides, no impurity peaks are presented in the XRD pattern, indicating that the coating of Fe_3O_4 core with ZrO_2 nanoparticles was successfully performed during the treatment process. The mean crystalline sizes of nano-Fe_3O_4@ZrO_2 nanoparticles for 2θ = 35.68° are calculated to be 13.26 nm using Debye-Scherrer equation, $t = 0.9\lambda/B_{1/2}\cos\theta$, where t is the average crystal size, λ is the wavelength of Cu-Ka (1.54 Å), $B_{1/2}$ is the angular line width at half maximum intensity and θ is the Bragg′s angle. As shown in Fig. 4c, nano-Fe_3O_4@ZrO_2/PMA represented the same patterns and intensity as those for nano-Fe_3O_4@ZrO_2 suggesting that after functionalization with PMA, the core-shell crystalline structure of the nanomaterial was maintained. However, in the diffractogram of nano-Fe_3O_4@ZrO_2/PMA no characteristic peaks of PMA can be detected. This indicates that heteropolyacid species are well-dispersed on the surface of nano-Fe_3O_4@ZrO_2 and there is not any crystalline phase of polyoxometalates in the resulted nanomaterials (Ghanbari-Siahkali et al., 2000; He et al., 2005). Meanwhile, the average crystal size of the as synthesized Fe_3O_4@ZrO_2/PMA nanocatalyst, with the aid of the Debye-Scherrer equation and the XRD results, for 2θ = 35.62° is determined to be around 17 nm.

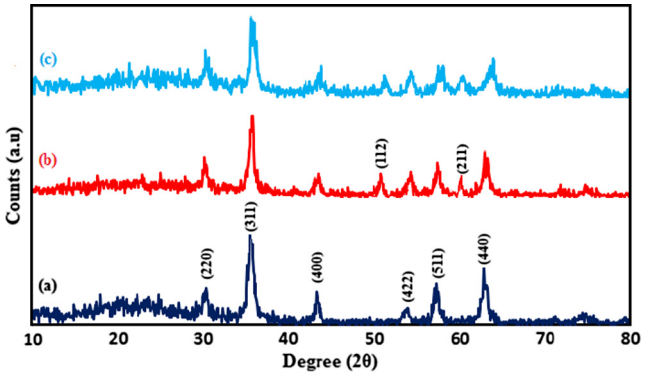

Figure 4 XRD spectra of (a) nano-Fe_3O_4, (b) nano-Fe_3O_4@-ZrO_2 and (c) nano-Fe_3O_4@ZrO_2/PMA 20 wt.%.

3.4. Thermogravimetric analysis

In order to determine the thermal stability of the n-Fe_3O_4@ZrO_2 and n-Fe_3O_4@ZrO_2/PMA 20 wt.%, TGA analysis was employed (Fig. 5). According to Fig. 3a, the nano-Fe_3O_4@ZrO_2 support material represented a two-step decomposition. In the initial decomposition stage (at the temperatures under 120 °C), a weight loss of 1 wt.% was occurred which was due to the removal of physically adsorbed solvent and surface hydroxyl groups. The second steady mass loss (1 wt.%) at the temperatures below 800 °C possibly attributed to the dehydroxylation of ZrO_2. As shown in the curve 5b, Fe_3O_4@ZrO_2/PMA exhibited an entirely different TGA profile which approved grafting of PMA on the support material. In the thermogram of nano-Fe_3O_4@ZrO_2/PMA, a weight loss of about 2 wt.% taken place below 100 °C was ascribed to the loss of physisorbed water from the both support and heteropolyacid. The next loss of weight (about 2.5 wt.%) occurred between 150 and 300 °C possibly corresponded to the dehydroxylation of the chemisorbed water (Rocchiccioli-Deltcheff et al., 1992). The last steady slow thermal decomposition of the catalyst (around 1 wt.%) could be observed with the increase in the temperature up to 600 °C. This loss of weight was related to the evaporation of the crystalline water molecules in the heteropolyacid structure and decomposition of the Keggin units to give MoO_3 (El-Wahab and Said, 2005; Misono et al., 1982). Based on these findings, it was concluded that n-Fe_3O_4@ZrO_2/PMA was thermally stable and could tolerate the reactions operated up to 350 °C.

3.5. Field emission scanning electron microscopy

In order to analyze the morphology, size and distribution of n-Fe_3O_4@ZrO_2 and n-Fe_3O_4@ZrO_2/PMA, the FE-SEM analyses were employed (Fig. 6a–d). According to Fig. 6a and b, n-Fe_3O_4@ZrO_2 sample exhibited spherical particles. Besides, as it was obvious in Fig. 6c and d, the modified n-Fe_3O_4@ZrO_2 catalyst (i.e. n-Fe_3O_4@ZrO_2/PMA) displayed the same morphology as that of n-Fe_3O_4@ZrO_2. The n-Fe_3O_4@ZrO_2/PMA sample had the nearly homogeneous size distribution and morphology. However, during the process of functionalization, aggregation of the nanoparticles was observed.

3.6. Transmission electron microscopy (TEM)

Fig. 7a–d displays the TEM images of the Fe_3O_4@ZrO_2 and Fe_3O_4@ZrO_2/PMA MNPs. Fig. 7a shows that the average diameters for the spherical particles of Fe_3O_4@ZrO_2 MNPs were around 10–15 nm. As it appeared in the TEM images of Fe_3O_4@ZrO_2/PMA MNPs (FIg. 7b–d), the materials were comprised of spherical particles with the approximately homogenous size distribution. The average sizes of these nanoparticles were between 15 and 25 nm which showed a good matching with the values calculated by XRD analysis. These results confirmed that the functionalization of the Fe_3O_4@ZrO_2 MNPs was successfully performed with the enlargement in the particle diameters.

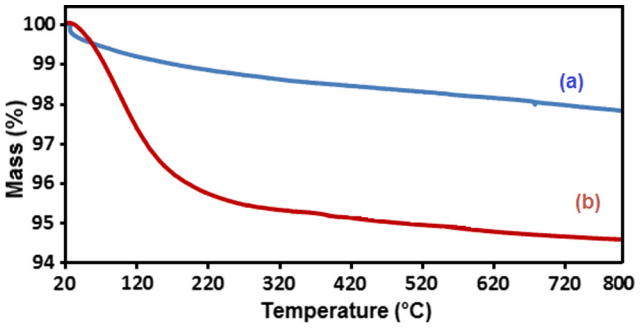

Figure 5 TGA curves of (a) n-Fe_3O_4@ZrO_2 and (b) n-Fe_3O_4@-ZrO_2/PMA 20 wt.%.

3.7. Energy dispersive X-ray (EDX) analysis

The elemental composition of the as-prepared catalyst was provided through EDX analysis. Fig. 8 displays the EDX spectrum of Fe_3O_4@ZrO_2/PMA MNPs which exhibited the presence of the elements as follows: Fe, Zr, O, Mo and P.

3.8. Vibrating sample magnetometer (VSM)

The samples of n-Fe_3O_4, n-Fe_3O_4@ZrO_2 and n-Fe_3O_4@ZrO_2/PMA were analyzed for their magnetic properties through a vibration sample magnetometer (VSM). As it could be observed from the loops (Fig. 9), the saturation magnetization values for n-Fe_3O_4, n-Fe_3O_4@ZrO_2 and n-Fe_3O_4@ZrO_2/PMA samples were 70.48, 53.52 and 35.97 emu g^{-1}, respectively. The decrease in the mass saturation magnetization in the last two samples was attributed to the presence of non-magnetic zirconia shell and the heteropolyacid groups. Although the Ms value of n-Fe_3O_4@ZrO_2/PMA material was lowered, its separation from the reaction mixture, using a magnetic stirring bar, could be efficient.

4. Experimental section

4.1. General consideration

All chemicals were purchased from Merck and Sigma-Aldrich companies and used without any further purification. The purity of products was checked by thin layer chromatography (TLC) on glass plates coated with silica gel 60 F254 using n-hexane/ethyl acetate mixture as mobile phase. Melting points were determined in open capillaries using an Electrothermal 9100 without further corrections. NMR spectra were recorded in pure deuterated acetone, chloroform and dimethyl sulfoxide with tetramethylsilane (TMS) as an internal standard at ambient temperature on Bruker Avance 300 MHz instruments (^{1}H NMR 300 MHz and ^{13}C NMR 75 MHz). Fourier transform infrared (FT-IR) spectra were provided on a Shimadzu 8400s spectrometer using KBr pressed powder disks. The crystal structure of synthesized materials was determined by an X-ray diffractometer (XRD) using a Cu-Kα radiation of wavelength 1.54 Å on a Siemens D5000 (Siemens AG, Munich, Germany) X-ray diffractometer. Thermogravimetric analyses (TGA) were performed on a Du Pont 2000 thermal analysis apparatus at a heating rate of 5 °C min^{-1} under air atmosphere. Scanning Electron Microscopy, SEM-EDX, analysis was carried out using Tescan Vega II XMU Digital Scanning Microscope. Transmission electron microscope, TEM (Philips – CM300 – 150 KV) was also used to acquire TEM images.

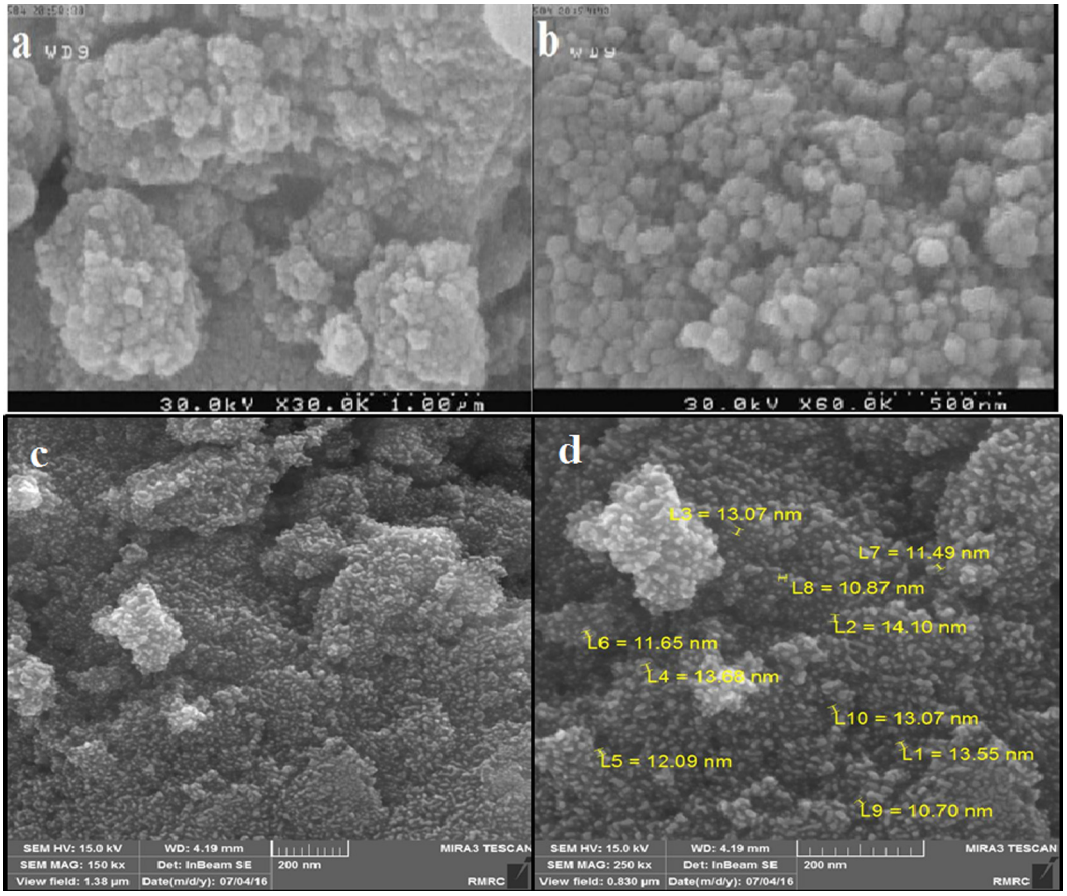

Figure 6 FE-SEM images of n-Fe_3O_4@ZrO_2 (a and b), and n-Fe_3O_4@ZrO_2/PMA (c and d).

Magnetic measurement was performed in a vibrating sample magnetometer (VSM) (4 inch, Daghigh Meghnatis Kashan Co., Kashan; Iran) at room temperature. All potentiometric measurements were performed with a digital multi-meter (Sinometer DM-97, China) using the glassy carbon disk electrode (2 mm diameter), as the indicator electrode in conjunction with an Ag/AgCl, (KCl 3 M) (Azar electrode, Iran) as reference electrode.

4.2. Synthesis of iron oxide magnetite nanoparticles

The Fe_3O_4 magnetite nanoparticles were prepared through a partial reduction coprecipitation method according to the reported procedure (Qu et al., 1999; Sun et al., 2004a). In brief, initially, 3 ml $FeCl_3$ (2 M dissolved in 2 M HCl) was added to the 10.33 ml double distilled water. Then, 2 ml Na_2SO_3 (1 M) was added to the former solution dropwise in 1 min while the solution was stirred vigorously. Just after the color of the solution altered from red to light yellow, the solution was added to the 80 ml $NH_3{\cdot}H_2O$ solution (0.85 M) under magnetic stirring. After 30 min, a black precipitates formed which were isolated by means of an external magnet and then washed with deionized water several times (to pH $<$ 7.5). The resulting black Fe_3O_4 MNPs were dried under vacuum at 60 °C for 12 h.

4.3. Preparation of Fe_3O_4@C magnetite nanoparticles

The Fe_3O_4@C MNPs were provided by the hydrothermal reaction of glucose on Fe_3O_4 MNPs according to the literature reported method (Li et al., 2007) with some modifications as follows:

At first, magnetite nanoparticles (100 mg) were suspended in 0.1 M HNO_3 (25 ml), sonicated for 20 min, isolated through external magnet and washed with deionized water. Then, the treated Fe_3O_4 nanoparticles were dispersed in aqueous glucose solution (0.5 M, 50 ml), stirred vigorously for 20 min and transferred into a 100-ml Teflon-lined stainless steel autoclave. Afterward, the autoclave was sealed and heated at 180 °C for 24 h. Subsequently, the autoclave was allowed to cool to room temperature and the created black suspensions were separated by means of a magnet and then, washed with deionized water and ethanol, three times. In the last step, after the over-night drying the sample at 80 °C, the desired Fe_3O_4@C magnetic nanoparticles were prepared.

4.4. Providing the core-shell Fe_3O_4@ZrO_2 nanoparticles

The core-shell Fe_3O_4@ZrO_2 MNPs were synthesized by means of a sonochemical route. In a typical synthetic experiment, zirconium (IV) oxychloride octahydrate ($ZrOCl_2{\cdot}8H_2O$) (0.3 g, 0.93 mmol) was firstly dissolved in ethanol (50 ml). When a clear solution formed, the Fe_3O_4@C MNPs (100 mg) were dispersed in this solution through ultrasonication for 20 min. While the suspension being sonicated during 15–20 min, a mixture of water and ethanol (1:5 v/v) was added dropwise and then again the suspension was allowed to vigorously be sonicated for another 2 h. After that, the suspended MNPs were

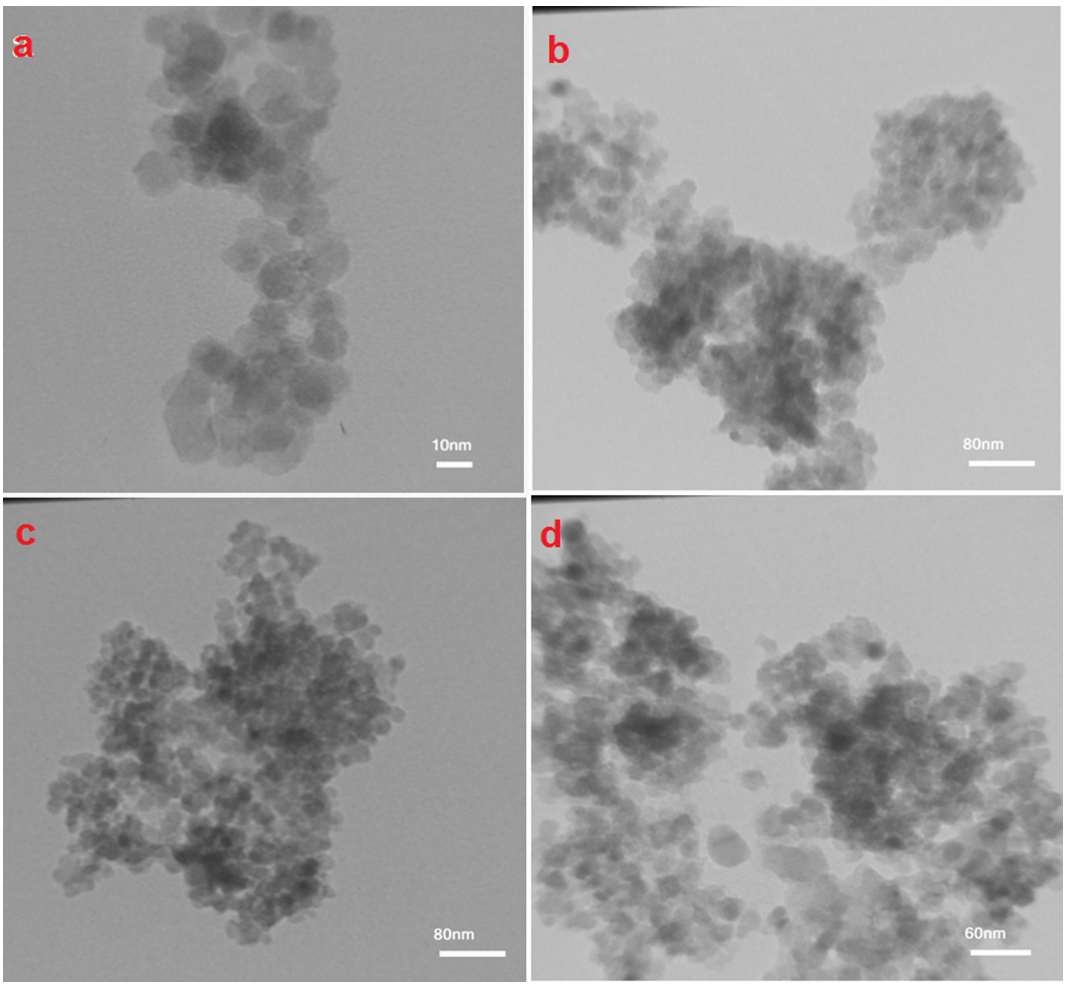

Figure 7 The TEM images of (a) n-Fe_3O_4@ZrO_2 and (b–d) n-Fe_3O_4@ZrO_2/PMA.

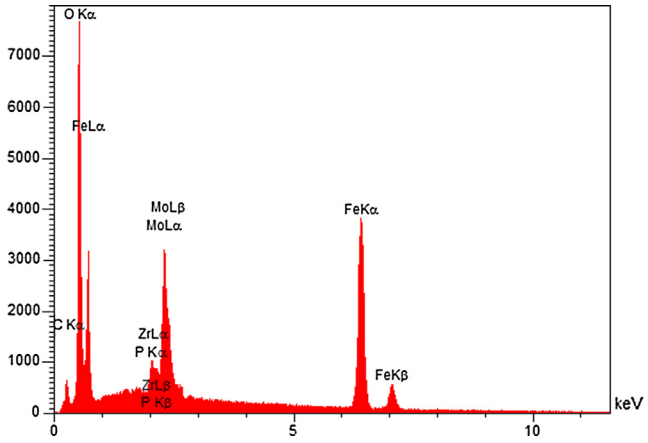

Figure 8 The EDX spectrum of n-Fe_3O_4@ZrO_2/PMA.

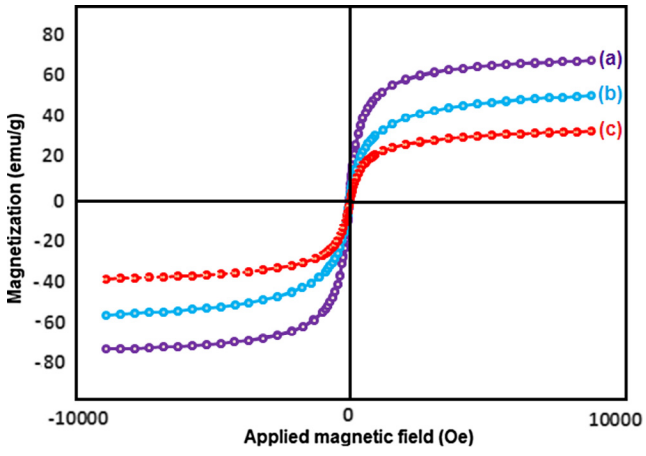

Figure 9 Magnetization curves of the (a) n-Fe_3O_4, (b) n-Fe_3O_4@ZrO_2 and (c) n-Fe_3O_4@ZrO_2/PMA.

separated through an external magnet and washed with ethanol, five times. In the final step, the Fe_3O_4@ZrO_2 nanoparticles were prepared after drying followed by calcination in air at 500 °C for 1 h.

4.5. Immobilization of phosphomolybdic acid on the core-shell Fe_3O_4@ZrO_2 nanoparticles

In order to prepare the Fe_3O_4@ZrO_2/PMA nanocatalysts with different loadings of 20 wt.%, at first, to the clear solution of

PMA (0.3 g) in double distilled water (5 ml), 1.0 g n-Fe_3O_4@ZrO_2 was dispersed through sonication for about 30 min. Afterward, the mixture was strongly stirred overnight at room temperature. After the removal of the water with the aid of rotary evaporator, the produced solid powder was dried at 60 °C for 24 h. In the last step, the desired nano-Fe_3O_4@ZrO_2/PMA of 1.35 g was prepared. Similar procedures were used for the synthesis of 10 and 30 wt.% of nano-Fe_3O_4@ZrO_2/PMA samples.

4.6. General procedure for the synthesis of 2, 4, 5-trisubstituted imidazoles

A mixture of aromatic aldehyde (1.0 mmol), benzil (1.0 mmol), ammonium acetate (2 mmol) and n-Fe_3O_4@ZrO_2/PMA (0.0025 g, 10 mol%) as catalyst was taken to a test tube equipped with a stir bar. The reaction was performed under solvent-free condition at 110 °C (in an oil bath) for the appropriate time until the completion of the reaction. The progress of the reaction was checked by thin layer chromatography (TLC) [7: 3 n-hexane: ethyl acetate]. After completion of the reaction (checked by TLC), hot ethanol (5 mL) was added and the catalyst was separated using an external magnet. After the filtrate was concentrated under rotary vacuum evaporation, the crude product recrystallized from ethanol to afford pure products. The products were confirmed through the comparison with authentic samples, IR, ^{1}H NMR spectra and melting points.

4.7. General procedure for the synthesis of 1, 2, 4, 5-tetrasubstituted imidazoles

A mixture of benzil (1 mmol), aldehyde (1 mmol), ammonium acetate (1 mmol), primary aromatic amine (1 mmol) and n-Fe_3O_4@ZrO_2/PMA (0.0025 g, 10 mol%) as catalyst was reacted in a test tube with a glass bar at 110 °C under solvent-free condition for the appropriate time. When the reaction was completed, checked by TLC, the reaction mixture was dissolved in ethanol (5 mL) and the catalyst was isolated by applying the magnetic field. Then, the filtrate was concentrated on a rotary evaporator under reduced pressure and the solid crude product created was washed with water and recrystallized from ethanol to afford pure products. The physical data (Mp, IR, and NMR) of all known compounds were identical with those reported in the literature.

4.8. Evaluation of the catalytic performance of n-Fe_3O_4@ZrO_2/PMA as heterogeneous acid nanocatalyst in the synthesis of multisubstituted imidazoles

After the Fe_3O_4@ZrO_2/PMA nanocatalyst was fully characterized by the aid of several techniques, its catalytic activity was investigated in the multicomponent reactions for the synthesis of 2, 4, 5-trisubstituted imidazoles from the reaction of aromatic aldehydes, benzil and NH_4OAc as well as for the preparation of 1, 2, 4, 5-tetrasubstituted imidazoles from the reaction of aromatic aldehydes, amines, benzil, and NH_4OAc under solvent free conditions.

4.9. Optimization of the reaction parameters for one-pot synthesis of 2, 4, 5-trisubstituted imidazoles

At the outset, we tested the reaction of benzaldehyde, benzil and NH_4OAc without any catalysts at 100 °C for the synthesis of 2, 4, 5-trisubstituted imidazole in the solvent-free condition. However, low yields of products were observed in the prolonged reaction time (Table 1, entry 1). In the subsequent step, with the aim of optimizing the reaction conditions, we examined the mentioned reaction in the presence of 5–20 mol% of nano-Fe_3O_4@ZrO_2/PMA as catalyst under solvent-free condition at 100 °C. The results indicated that 10 mol% of the catalyst was sufficient to yield 95% of the product in 15 min (Table 1, entries 2–5). Compared to reactions carried out in the presence of nano-Fe_3O_4@ZrO_2/PMA, the reaction catalyzed by unfunctionalized nano-Fe_3O_4@ZrO_2 afforded lower yields of the desired product. Based on this fact, it was deduced that the employment of nano-Fe_3O_4@ZrO_2/PMA catalyst in the reaction was essential. The superior catalytic activity of nano-Fe_3O_4@ZrO_2/PMA catalyst was most probably ascribed to the immobilization of the strong super acid (PMA) on the surface of the nano-Fe_3O_4@ZrO_2, which could offer a large numbers of BrØnsted acid sites. After the optimum catalyst loading was determined, the model reaction was investigated through adding of nano-Fe_3O_4@ZrO_2/PMA (10 mol%) as catalyst under solvent free condition in the different temperatures (80, 90, 100, 110, and 120 °C), because temperature is an important factor for the synthesis of imidazole compounds (Table 1, entries 3 and 6–9). According to Table 1, by increasing the temperature to 120 °C, a reduction in the reaction time was observed to 8 min, but the product yields were similar to those at the 110 °C; therefore, the most efficient reaction temperature was 110 °C which provided 98% of product yields within 10 min (Table 1, entry 7). In order to study the solvent effects on the model reaction, various solvents such as MeOH, EtOH, CH_3CN, CH_2Cl_2, and H_2O were employed in the reaction condition. As it was clear in Table 1 (Entries 10–14), with applying these solvents, lower yields of products were rendered. Therefore, solvent-free reaction condition, as the best condition, was selected to be in line with the green chemistry protocols. Consequently, the optimized reaction parameters, which we proposed, were 110 °C, 10 mol% of the nano-Fe_3O_4@ZrO_2/PMA catalyst, and solvent-free conditions (Table 1, entry 7). Finally, the scope of the reaction was further extended under the established optimal conditions (Scheme 2). As exhibited in Table 2, a wide variety of aromatic aldehydes including electron-rich (deactivated) and electron-deficient (activated) were reacted with benzil and ammonium acetate which provided the corresponding 2, 4, 5-trisubstituted imidazoles in good yields (Table 2). It was noteworthy that aldehydes bearing either electron-withdrawing or electron-donating groups performed equally well in the reaction. The nature and position of the substituents on the aromatic aldehyde had no significant effect on the reaction yields (Table 2).

4.10. Synthesis of tetrasubstituted imidazole derivatives

The above-mentioned promising results prompted us to further extend the scope of the catalytic activity of

Table 1 Optimization of the reaction condition for the synthesis of 2, 4, 5-trisubstituted imidazoles.[a]

Entry	Solvent	Condition	Catalyst (mmol)	Time (min)	Yield (%)
1	Solvent-free	100 °C	–	120	70
2	Solvent-free	100 °C	0.05	15	93
3	Solvent-free	100 °C	0.1	15	95
4	Solvent-free	100 °C	0.15	15	96
5	Solvent-free	100 °C	0.2	15	91
6	Solvent-free	120 °C	0.1	8	98
7	Solvent-free	110 °C	0.1	10	98
8	Solvent-free	90 °C	0.1	30	91
9	Solvent-free	80 °C	0.1	50	88
10	H_2O	Reflux	0.1	10	70
11	CH_3CN	Reflux	0.1	10	72
12	CH_2Cl_2	Reflux	0.1	10	68
13	EtOH	Reflux	0.1	10	83
14	MeOH	Reflux	0.1	10	79

[a] Reaction condition: benzil (1 mmol), benzaldehyde (1 mmol), and NH_4OAc (2 mmol).

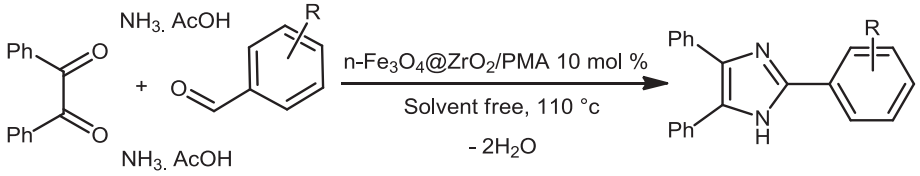

Scheme 2 Synthesis of 2, 4, 5-trisubstituted imidazoles in the optimum condition.

Table 2 n-Fe_3O_4@ZrO_2/PMA-catalyzed one-pot synthesis of 2, 4, 5-trisubstituted imidazoles.[a]

Entry	R	*T* (min)	Yield (%)[b]	Mp (°C)
1	-H	10	98	271–273 (Kidwai et al., 2007)
2	2-Cl	15	85	200–201 (Wang et al., 2009)
3	4-Cl	20	96	262–263 (Kidwai et al., 2007)
4	2,4-$(Cl)_2$	12	95	176–177 (Khosropour, 2008)
5	3-Br	40	90	304–305 (Nemati et al., 2013)
6	3-NO_2	45	84	265–266 (Kidwai et al., 2007)
7	4-NO_2	30	88	231–233 (Zang et al., 2010)
8	2-OCH_3	35	85	210–211 (Bamoniri et al., 2014)
9	4-OCH_3	30	89	230–232 (Joshi et al., 2010)
10	2-OH	30	91	211–212 (Wang et al., 2006)
11	3-OH	25	93	258 (Azizi et al., 2012)
12	4-OH	15	95	257–259 (Kidwai et al., 2007)
13	4-CH_3	20	94	227–228 (Kidwai et al., 2007)
14	3-OEt, 4-OH	55	93	267–268 (Nemati et al., 2013)
15	3,4-$(OMe)_2$	25	91	220–222 (Marzouk et al., 2013)
16	4-$N(CH_3)_2$	40	80	256–237 (Safari et al., 2010)
17	4-$CH(CH_3)_2$	35	93	252–255 (Mirjalili et al., 2013)

[a] Reaction condition: benzil (1 mmol), aromatic aldehyde (1 mmol), NH_4OAc (2 mmol) and n-Fe_3O_4@ZrO_2/PMA (0.1 mmol), solvent-free, 110 °C.
[b] Yields refer to isolated products.

n-Fe_3O_4@ZrO_2/PMA for the synthesis of tetrasubstituted imidazoles through the one-pot four-component condensation of benzil (1 mmol), aromatic aldehyde (1 mmol), ammonium acetate (1 mmol), primary aromatic amine (1 mmol) and n-Fe_3O_4@ZrO_2/PMA (10 mol%) as catalyst under the optimized condition (i.e. 110 °C, 10 mol% of the catalyst, and solvent-free condition), (Scheme 3).

In order to show the effectiveness and advantages of the designed catalyst, its catalytic performance was compared to some previous methods for the synthesis of 1, 2, 4,

Table 3 n-Fe_3O_4@ZrO_2/PMA-catalyzed one-pot synthesis of 1, 2, 4, 5-tetrasubstituted imidazoles.[a]

Entry	R_1	R_2	*T* (min)	Yield (%)[b]	Mp (°C)
1	-H	-H	50	93	217–218 (Heravi et al., 2007)
2	4-CH_3	-H	80	96	189–191 (Heravi et al., 2007)
3	4-OCH_3	-H	100	91	181–183 (Karimi et al., 2010)
4	3-OH	-H	45	89	230–232
5	4-OH	-H	60	82	281–282 (Sadeghi et al., 2011)
6	4-NO_2	-H	80	87	185–187 (Karimi et al., 2010)
7	4-Cl	-H	70	91	163–164 (Murthy et al., 2010)
8	2,6-$(Cl)_2$	-H	45	93	256–258
9	4-Cl	4-Cl	135	82	188–190 (Nagarapu et al., 2007)
10	4-CH_3	4-Cl	135	86	165–167 (Karimi et al., 2010)
11	3-NO_2	4-CH_3	80	84	150–152 (Kantevari et al., 2007)
12	4-NO_2	4-CH_3	60	89	220–222 (Kantevari et al., 2007)
13	4-OH	4-CH_3	100	91	278–280 (Nagarapu et al., 2007)
14	4-CH_3	4-CH_3	90	94	188–190 (Kantevari et al., 2007)

[a] Reaction condition: benzil (1 mmol), aromatic aldehyde (1 mmol), NH_4OAc (1 mmol), aromatic amine (1 mmol) and n-Fe_3O_4@ZrO_2/PMA (0.1 mmol), solvent-free, 110 °C.
[b] Yields refer to isolated products.

Table 4 Comparison of the efficiency of n-Fe_3O_4@ZrO_2/PMA with different catalysts reported before for the synthesis of 1, 2, 4, 5-tetrasubstituted imidazoles.

Entry	Catalyst	Condition	Time (min)	Yield (%)	Ref.
1	Nano-crystalline SZ[a]	Reflux in EtOH	45	87	Teimouri and Chermahini (2011)
2	WD[b]/SiO_2	Solvent-free/140 °C	120	85	Karimi et al. (2010)
3	$MgCl_2$	Solvent-free/80 °C	45	60	Sadeghi et al. (2011)
4	Bf_3/SiO_2	Solvent-free/140 °C	120	92	Sadeghi et al. (2008)
5	Zeolite	Reflux in EtOH	60	80	Teimouri and Chermahini (2011)
6	$NaHSO_4/SiO_2$	Solvent-free/140 °C	120	92	Karimi et al. (2006)
7	$SbCl_5/SiO_2$	Solvent-free/140 °C	120	90	Sadeghi et al. (2011)
8	Montmorilonite K10	Reflux in EtOH	90	75	Teimouri and Chermahini (2011)
9	$[(CH_2)_4SO_3HMIM][HSO_4]$	Solvent-free/140 °C	150	88	Davoodnia et al. (2010)
10	$H_3PMo_{12}O_{40}$	Reflux in EtOH	15	88	Heravi et al. (2007)
11	$K_7Na_3P_2W_{18}Cu_4O_{68}$	CH_2Cl_2/140 °C	90	87	Kalkhorani and Heravi (2013)
12	n-Fe_3O_4@ZrO_2/PMA	Solvent-free/110 °C	50	93	Present work

[a] Sulfated zirconia.
[b] Wells–Dawson heteropolyacid supported on silica.

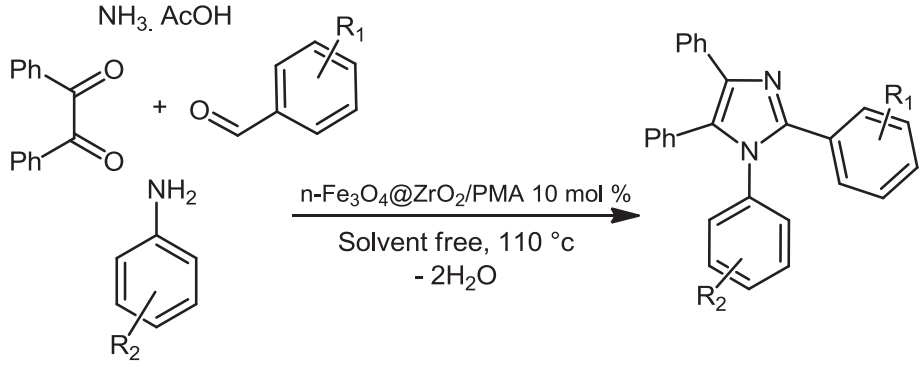

Scheme 3 Synthesis of 1, 2, 4, 5-tetrasubstituted imidazoles in the optimum condition.

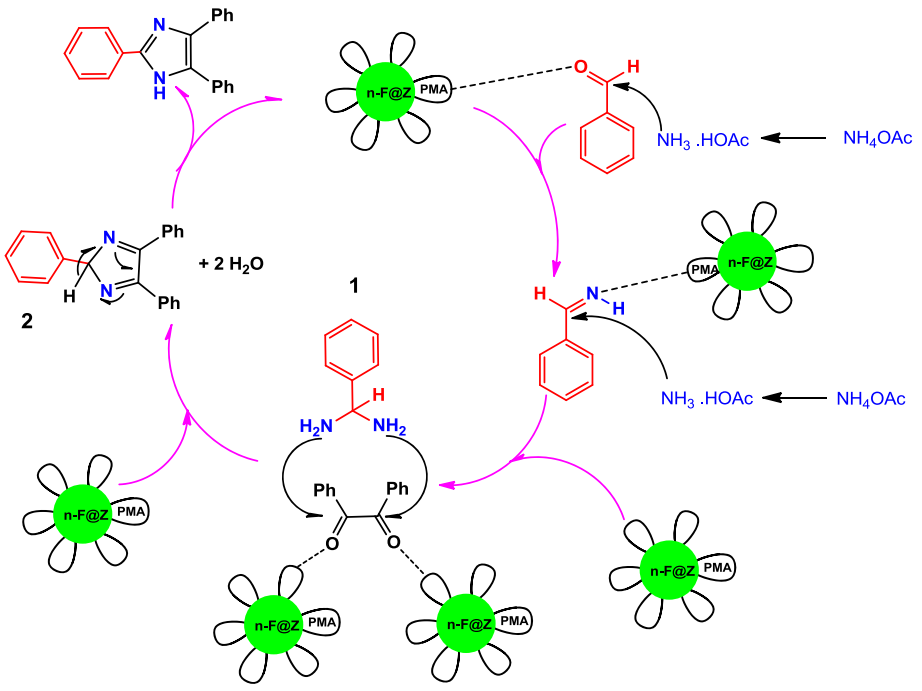

Scheme 4 Possible mechanism for the synthesis of 2, 4, 5-trisubstituted imidazole in the presence of n-Fe_3O_4@ZrO_2/PMA.

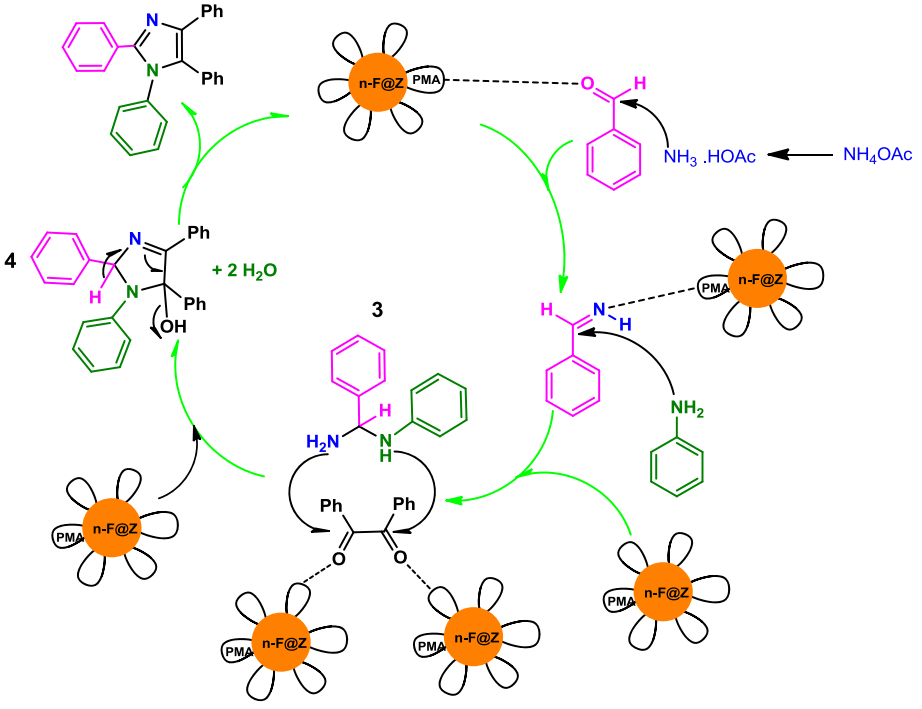

Scheme 5 Proposed mechanism for the synthesis of 1, 2, 4, 5-tetrasubstituted imidazole catalyzed by n-Fe_3O_4@ZrO_2/PMA.

5-tetrasubstituted imidazoles (Table 4). As it was obvious, the n-Fe_3O_4@ZrO_2/PMA catalyst was superior to the other mentioned catalytic systems regarding easy separability, high activity and reusability in addition to higher reaction efficiency and shorter reaction time. These results verified the high efficiency of n-Fe_3O_4@ZrO_2/PMA (see Table 3).

4.11. Plausible mechanism for the synthesis of 2, 4, 5-trisubstituted and 1, 2, 4, 5-tetrasubstituted imidazoles catalyzed by n-Fe_3O_4@ZrO_2/PMA

The possible mechanism for n-Fe_3O_4@ZrO_2/PMA catalyzed production of trisubstituted imidazole was shown in Scheme 4.

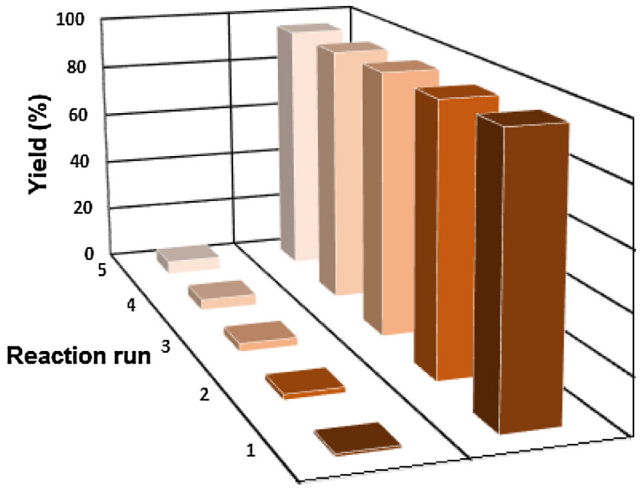

Run	1	2	3	4	5
Yield [%]	98	97	97	96	96

Figure 10 Reusability of n-Fe_3O_4@ZrO_2/PMA for the synthesis of 2, 4, 5-trisubstituted imidazole.

At first, diamine intermediate 1 was generated through the condensation reaction of aldehyde with the two equivalent of ammonia (formed by the dissociation of ammonium acetate) in the presence of the catalyst. Afterward, intermediate 2 was formed by the reaction of intermediate 1 with benzil, which in turn rearranged to the trisubstituted imidazole. Similarly, the probable mechanism for the synthesis of tetrasubstituted imidazoles started with the formation of intermediate 3 by the reaction of an aldehyde, phenyl amine and ammonium acetate which was mediated with the catalyst. Intermediate 4 was formed by condensing intermediate 3 with benzil, which produced the tetrasubstituted imidazole after (Scheme 5).

4.12. Recycling experiments

For designing a greener process, the capability of the used catalyst in terms of recovery and reuse, for several times, should be taken seriously. With respect to the matter, we investigated the level of recyclability of the n-Fe_3O_4@ZrO_2/PMA catalyst in the model aforementioned reaction condition for the synthesis of multisubstituted imidazole. After the reactions were ended, the catalyst was removed from the mixtures by an external magnet. Then the remaining catalyst was washed with ethanol and water to remove the residual product. When dried under vacuum, the recovered catalyst was ready to employ in the reaction mixture of fresh reactants under same conditions. According to the data obtained from the recycling tests, the catalyst could be reused for five runs with no remarkable drop in yield and its catalytic activity (Fig. 10). Additionally, to perform the leaching experiments, the model reaction for the synthesis of tetrasubstituted imidazole was carried out in the mentioned optimum reaction condition. After 10 min the catalyst was removed by an external magnet. Then the residual solution continued to react. However no significant progress in the reaction was seen even in prolonged time. From this observation, it could be concluded that the PMA functions were tightly immobilized on the surface of n-Fe_3O_4@ZrO_2 support.

5. Conclusion

Phosphomolybdic acid (PMA) was covalently immobilized on the surface of n-Fe_3O_4@ZrO_2 to produce the heterogeneous highly powerful Fe_3O_4@ZrO_2/PMA catalyst in nano-size. The introduced strong solid acid was proved to be an excellent catalyst in the simple, efficient, and rapid one-pot three- and four-component reactions for the synthesis of multisubstituted imidazoles. In addition, this efficient and environmentally friendly Brønsted acidic catalyst was easily isolated from the reaction mixture under a magnetic field and efficiently reused for further cycles of transformation, retaining its high productivity in the 5th reaction cycle. As a consequence, the outstanding recyclability and reusability, facile magnetically separability, significant stability, high reaction efficiency and short reaction times could cause the catalyst to be economical and industrially interesting.

Acknowledgments

The authors would like to thank Semnan University Research Council for the financial support of this work.

References

Antolini, M., Bozzoli, A., Ghiron, C., Kennedy, G., Rossi, T., Ursini, A., 1999. Analogues of 4,5-bis(3,5-dichlorophenyl)-2-trifluoromethyl-1H-imidazole as potential antibacterial agents. Bioorg. Med. Chem. Lett. 9, 1023–1028.

Azizi, N., Dado, N., Amiri, A.K., 2012. Highly efficient one-pot synthesis of trisubstituted imidazoles under catalyst-free conditions. Can. J. Chem. 90, 195–198.

Bamoniri, A., Mirjalili, B.F., Nazemian, S., Mahabadi1, N.Y., 2014. Nano silica phosphoric acid as an efficient catalyst for one-pot synthesis of 2,4,5-trisubstituted imidazoles under solvent free condition. Bulg. Chem. Commun. 46, 79–84.

Bossche, H.V.D., Willemsens, G., Cools, W., Marichal, P., Lauwers, W., 1983. Hypothesis on the molecular basis of the antifungal activity of N-substituted imidazoles and triazoles. Biochem. Soc. Trans. 11, 665–667.

Caló, V., Nacci, A., Monopoli, A., Laera, S., Cioffi, N., 2003. Pd nanoparticles catalyzed stereospecific synthesis of β-aryl cinnamic esters in ionic liquids. J. Org. Chem. 68, 2929–2933.

Cave, G.W.V., Raston, C.L., Scott, J.L., 2001. Recent advances in solventless organic reactions: towards benign synthesis with remarkable versatility. Chem. Commun., 2159–2169

Chen, M., Yamamuro, S., Farrell, D., Majetich, S.A., 2003. Gold-coated iron nanoparticles for biomedical applications. J. Appl. Phys. 93, 7551–7553.

Chen, Z., Xue, Z., Chen, L., Geng, Z., Yang, R., Chen, L., Wang, Z., 2013. One-pot template-free synthesis of water-dispersive Fe_3O_4@-C nanoparticles for adsorption of bovine serum albumin. New J. Chem. 37, 3731–3736.

Clark, J.H., 2002. Solid acids for green chemistry. Acc. Chem. Res. 35, 791–797.

Corma, A., Martínez, A., 1993. Chemistry, catalysts, and processes for isoparaffin–olefin alkylation: actual situation and future trends. Catal. Rev. Sci. Eng. 35, 483–570.

Damyanova, S., Fierro, J.L.G., Sobrados, I., Sanz, J., 1999. Surface behavior of supported 12-heteropoly acid as revealed by nuclear magnetic resonance, X-ray photoelectron spectroscopy, and Fourier transform infrared techniques. Langmuir 15, 469–476.

Davoodnia, A., Heravi, M.M., Safavi-Rad, Z., Tavakoli-Hoseini, N., 2010. Green, one-pot, solvent-free synthesis of 1, 2, 4, 5-tetrasubstituted imidazoles using a Brønsted acidic ionic liquid as novel and reusable catalyst. Synth. Commun. 40, 2588–2597.

Deprez, P., Mandine, E., Vermond, A., Lesuisse, D., 2002. Imidazole-based ligands of the Src SH_2 protein. Bioorg. Med. Chem. Lett. 12, 1287–1289.

El-Wahab, M.M.M.A., Said, A.A., 2005. Phosphomolybdic acid supported on silica gel and promoted with alkali metal ions as catalysts for the esterification of acetic acid by ethanol. J. Mol. Catal. A: Chem. 240, 109–118.

Feyen, M., Weidenthaler, C., Schüth, F., Lu, A.H., 2010. Synthesis of structurally stable colloidal composites as magnetically recyclable acid catalysts. Chem. Mater. 22, 2955–2961.

Freedman, J.E., Loscalzo, J., 2009. New Therapeutic Agents in Thrombosis and Thrombolysis. CRC Press.

Gallagher, T.F., Fier-Thompson, S.M., Garigipati, R.S., Sorenson, M. E., Smietana, J.M., Lee, D., Bender, P.E., Lee, J.C., Laydon, J.T., Griswold, D.E., Chabot-Fletcher, M.C., Breton, J.J., Adams, J.L., 1995. 2,4,5-triarylimidazole inhibitors of IL-1 biosynthesis. Bioorg. Med. Chem. Lett. 5, 1171–1176.

Ghanbari-Siahkali, A., Philippou, A., Dwyer, J., Anderson, M.W., 2000. The acidity and catalytic activity of heteropoly acid on MCM-41 investigated by MAS NMR, FTIR and catalytic tests. Appl. Catal. A 192, 57–69.

Gill, C.S., Price, B.A., Jones, C.W., 2007. Sulfonic acid-functionalized silica-coated magnetic nanoparticle catalysts. J. Catal. 251, 145–152.

He, N.Y., Woo, C.S., Kim, H.G., Lee, H.I., 2005. Catalytic formation of acetic anhydride over tungstophosphoric acid modified SBA-15 mesoporous materials. Appl. Catal. A 281, 167–178.

Heravi, M.M., Derikvand, F., Bamoharram, F.F., 2007. Highly efficient, four-component one-pot synthesis of tetrasubstituted imidazoles using Keggin-type heteropolyacids as green and reusable catalysts. J. Mol. Catal. A: Chem. 263, 112–114.

Hosseini, M.M., Kolvari, E., Koukabi, N., Ziyaei, M., Zolfigol, M.A., 2016. Zirconia sulfuric acid: an efficient heterogeneous catalyst for the one-pot synthesis of 3, 4-dihydropyrimidinones under solvent-free conditions. Catal. Lett. 146, 1040–1049.

Izumi, Y., Ono, M., Ogawa, M., Urabe, K., 1993. Acidic cesium salts of Keggin-type heteropolytungstic acids as insoluble solid acid catalysts for esterification and hydrolysis reactions. Chem. Lett., 825–828

Joshi, R.S., Mandhane, P.G., Shaikh, M.U., Kale, R.P., Gill, C.H., 2010. Potassium dihydrogen phosphate catalyzed one-pot synthesis of 2, 4, 5-triaryl-1*H*-imidazoles. Chin. Chem. Lett. 21, 429–432.

Kalkhorani, N.M., Heravi, M.M., 2013. K_7Na_3 P_2 W_{18} Cu $_4$ O_{68}: A mild, efficient, and reusable catalyst for the one-pot synthesis of 1, 2, 4, 5-tetra substituted imidazoles. J. Chem.

Kantevari, S., Vuppalapati, S.V.N., Biradar, D.O., Nagarapu, L., 2007. Highly efficient, one-pot, solvent-free synthesis of tetrasubstituted imidazoles using $HClO_4$–SiO_2 as novel heterogeneous catalyst. J. Mol. Cat. A: Chem. 266, 109–113.

Karimi, A.R., Alimohammadi, Z., Amini, M.M., 2010. Wells-Dawson heteropoly acid supported on silica: a highly efficient catalyst for synthesis of 2,4,5-trisubstituted and 1,2,4,5-tetrasubstituted imidazoles. Mol. Diversity 14, 635–641.

Karimi, A.R., Alimohammadi, Z., Azizian, J., Mohammadi, A.A., Mohammadizadeh, M.R., 2006. Solvent-free synthesis of tetrasubstituted imidazoles on silica gel/$NaHSO_4$ support. Catal. Commun. 7, 728–732.

Kašpar, J., Fornasiero, P., Hickey, N., 2003. Automotive catalytic converters: current status and some perspectives. Catal. Today 77, 419–449.

Khosropour, A.R., 2008. Ultrasound-promoted greener synthesis of 2,4,5-trisubstituted imidazoles catalyzed by $Zr(acac)_4$ under ambient conditions. Ultrason. Sonochem. 15, 659.

Kidwai, M., Mothsra, P., Bansal, V., Somvanshi, R.K., Ethayathulla, A.S., Dey, S., Singh, T.P., 2007. One-pot synthesis of highly substituted imidazoles using molecular iodine: a versatile catalyst. J. Mol. Catal. A: Chem. 265, 177–182.

Kim, H.J., Shul, Y.G., Han, H., 2006. Synthesis of heteropolyacid ($H_3PW_{12}O_{40}$)/SiO_2 nanoparticles and their catalytic properties. Appl. Catal. A: Gen. 299, 46–51.

Kolvari, E., Koukabi, N., Armandpour, O., 2014. A simple and efficient synthesis of 3,4-dihydropyrimidin-2-(1*H*)-ones via Biginelli reaction catalyzed by nanomagnetic-supported sulfonic acid. Tetrahedron 70, 1383–1386.

Kolvari, E., Koukabi, N., Hosseini, M.M., 2015a. Perlite: A cheap natural support for immobilization of sulfonic acid as a heterogeneous solid acid catalyst for the heterocyclic multicomponent reaction. J. Mol. Catal. A: Chem. 397, 68–75.

Kolvari, E., Koukabi, N., Hosseini, M.M., Khandani, Z., 2015b. Perlite: an inexpensive natural support for heterogenization of HBF_4. RSC Adv. 5, 36828–36836.

Kolvari, E., Koukabi, N., Hosseini, M.M., Vahidian, M., Ghobadi, E., 2016. Nano-ZrO_2 sulfuric acid: a heterogeneous solid acid nano catalyst for Biginelli reaction under solvent free conditions. RSC Adv. 6, 7419–7425.

Kolvari, E., Zolfagharinia, S., 2016. A waste to wealth approach through utilization of nano-Ceramic Tile Waste as an accessible and inexpensive solid support to produce a heterogeneous solid acid nanocatalyst: To kill three birds with one stone. RSC Adv. 6, 93963–93974.

Koukabi, N., Kolvari, E., Khazaei, A., Zolfigol, M.A., Shaghasemi, B. S., Khavasi, H.R., 2011. Hantzsch reaction on free nano-Fe_2O_3 catalyst: excellent reactivity combined with facile catalyst recovery and recyclability. Chem. Commun. 47, 9230–9232.

Koukabi, N., Kolvari, E., Zolfigol, M.A., Khazaei, A., Shaghasemi, B. S., Fasahatib, B., 2012. A magnetic particle-supported sulfonic acid catalyst: tuning catalytic activity between homogeneous and heterogeneous catalysis. Adv. Synth. Catal. 354, 2001–2008.

Kozhevnikov, I.V., 1998. Catalysis by heteropoly acids and multicomponent polyoxometalates in liquid-phase reactions. Chem. Rev. 98, 171–198.

Kumar, A.P., Kim, J.H., Thanh, T.D., Lee, Y.I., 2013. Chiral zirconia magnetic microspheres as a new recyclable selector for the discrimination of racemic drugs. J. Mater. Chem. B 1, 4909–4915.

Lange, J.H., Stuivenberg, H.H.V., Coolen, H.K., Adolfs, T.J., McCreary, A.C., Keizer, H.G., Wals, H.C., Veerman, W., Borst, A.J., Looff, W.D., Verveer, P.C., Kruse, C.G., 2005. Bioisosteric replacements of the pyrazole moiety of rimonabant: synthesis, biological properties, and molecular modeling investigations of thiazoles, triazoles, and imidazoles as potent and selective CB1 cannabinoid receptor antagonists. J. Med. Chem. 48, 1823–1838.

Laszlo, S.E.D., Hacker, C., Li, B., Kim, D., MacCoss, M., Mantlo, N., Pivnichny, J.V., Colwell, L., Koch, G.E., Cascieri, M.A., Hagmann, W.K., 1999. Potent, orally absorbed glucagon receptor antagonists. Bioorg. Med. Chem. Lett. 9, 641–646.

Li, Y., Leng, T., Lin, H., Deng, C., Xu, X., Yao, N., Yang, P., Zhang, X., 2007. Preparation of Fe_3O_4@ZrO_2 core-shell microspheres as affinity probes for selective enrichment and direct determination of phosphopeptides using matrix-assisted laser desorption ionization mass spectrometry. J. Proteome Res. 6, 4498–4510.

Lim, C.W., Lee, I.S., 2010. Magnetically recyclable nanocatalyst systems for the organic reactions. Nano Today 5, 412–434.

Long, D.L., Tsunashima, R., Cronin, L., 2010. Polyoxometalates: building blocks for functional nanoscale systems. Angew. Chem. Int. Ed. 49, 1736–1758.

Mallik, S., Dash, S.S., Parida, K.M., Mohapatra, B.K., 2006. Synthesis, characterization, and catalytic activity of phosphomolybdic acid supported on hydrous zirconia. J. Colloid Interface Sci. 300, 237–243.

Marzouk, A.A., Abbasov, V.M., Talybov, A.H., Mohamed, S.K., 2013. Synthesis of 2,4,5-triphenyl imidazole derivatives using diethyl ammonium hydrogen phosphate as green, fast and reusable catalyst. WJOC 1, 6–10.

Mévellec, V., Roucoux, A., Ramirez, E., Philippot, K., Chaudret, B., 2004. Surfactant-stabilized aqueous iridium (0) colloidal suspension: an efficient reusable catalyst for hydrogenation of arenes in biphasic media. Adv. Synth. Catal. 346, 72–76.

Mirjalili, B., Bamoniri, A., Mohaghegh, N., 2013. One-pot synthesis of 2,4,5-tri-substituted-1*H*-imidazoles promoted by trichloromelamine. Curr. Chem. Lett. 2, 35–42.

Misono, M., Mizuno, N., Katamura, K., Kasai, A., Konishi, Y., Sakata, K., Okuhara, T., Yoneda, Y., 1982. Catalysis by heteropoly compounds. III. The structure and properties of 12-heteropolyacids of molybdenum and tungsten ($H_3PMo_{12-x}W_xO_{40}$) and their salts pertinent to heterogeneous catalysis. Bull. Chem. Soc. Jpn 55, 400–406.

Misono, M., Okuhara, T., 1993. Solid superacid catalysts. ChemTech 23.

Mitsutani, A., 2002. Future possibilities of recently commercialized acid/base-catalyzed chemical processes. Catal. Today 73, 57–63.

Mizuno, N., Yamaguchi, K., Kamata, K., 2011. Molecular design of polyoxometalate-based compounds for environmentally-friendly functional group transformations: from molecular catalysts to heterogeneous catalysts. Catal. Surv. Asia 15, 68–79.

Murthy, S.N., Madhav, B., Nageswar, Y.V.D., 2010. DABCO as a mild and efficient catalytic system for the synthesis of highly substituted imidazoles via multi-component condensation strategy. Tetrahedron Lett. 51, 5252–5257.

Nagarapu, L., Apuri, S., Kantevari, S., 2007. Potassium dodecatugstocobaltate trihydrate ($K_5CoW_{12}O_{40}{\cdot}3H_2O$): a mild and efficient reusable catalyst for the one-pot synthesis of 1, 2, 4, 5-tetrasubstituted imidazoles under conventional heating and microwave irradiation. J. Mol. Cat. A: Chem. 266, 104–108.

Narayanan, R., El-Sayed, M.A., 2003. Effect of catalysis on the stability of metallic nanoparticles: Suzuki reaction catalyzed by PVP-palladium nanoparticles. J. Am. Chem. Soc. 125, 8340–8347.

Nemati, F., Hosseini, M.M., Kiani, H., 2013. Glycerol as a green solvent for efficient, one-pot and catalyst free synthesis of 2,4,5-triaryl and 1,2,4,5-tetraaryl imidazole derivatives. J. Saudi Chem. Soc.

Okuhara, T., 2003. Microporous heteropoly compounds and their shape selective catalysis. Appl. Catal. A: Gen. 256, 213–224.

Pujari, S.P., Scheres, L., Marcelis, A., Zuilhof, H., 2014. Covalent surface modification of oxide surfaces. Angew. Chem. Int. Ed. 53, 6322–6356.

Qu, S., Yang, H., Ren, D., Kan, S., Zou, G., Li, D., Li, M., 1999. Magnetite nanoparticles prepared by precipitation from partially reduced ferric chloride aqueous solutions. J. Colloid Interface Sci. 215, 190–192.

Rafiee, E., Joshaghani, M., Eavani, S., Rashidzadeh, S., 2008. A revision for the synthesis of β-enaminones in solvent free conditions: efficacy of different supported heteropoly acids as active and reusable catalysts. Green Chem. 10, 982–989.

Rao, G.R., Rajkumar, T., Varghese, B., 2009. Synthesis and characterization of 1-butyl 3-methyl imidazolium phosphomolybdate molecular salt. Solid State Sci. 11, 36–42.

Rocchiccioli-Deltcheff, C., Amirouche, M., Fournier, M., 1992. Structure and catalytic properties of silica-supported polyoxomolybdates III. 12-molybdosilicic acid catalysts: vibrational study of the dispersion effect and nature of the Mo species in interaction with the silica support. J. Catal. 138, 445–456.

Rossi, L.M., Costa, N.J.S., Silva, F.P., Wojcieszak, R., 2014. Magnetic nanomaterials in catalysis: advanced catalysts for magnetic separation and beyond. Green Chem. 16, 2906–2933.

Sadeghi, B., Mirjalili, B.B.F., Bidaki, S., Ghasemkhani, M., 2011. Ghasemkhani, M. $SbCl_5.SiO_2$: an efficient alternative for one-pot synthesis of 1,2,4,5-tetrasubstituted imidazoles in solvent or under solvent-free condition. J. Iran Chem. Soc. 8, 648–652.

Sadeghi, B., Mirjalili, B.B.F., Hashemi, M., 2008. $BF_3{\cdot}SiO_2$: an efficient reagent system for the one-pot synthesis of 1,2,4,5-tetrasubstituted imidazoles. Tetrahedron Lett. 49, 2575–2577.

Safari, J., Khalili, S.D., Rezaei, M., Banitaba, S.H., 2010. A novel and an efficient catalyst for one-pot synthesis of 2,4,5-trisubstituted imidazoles by using microwave irradiation under solvent-free conditions. J. Chem. Sci. 122, 437–441.

Sarkar, A., Biswas, S.K., Pramanik, P., 2010. Design of a new nanostructure comprising mesoporous ZrO_2 shell and magnetite core (Fe_3O_4@mZrO_2) and study of its phosphate ion separation efficiency. J. Mater. Chem. 20, 4417–4424.

Sarshar, S., Zhang, C., Moran, E.J., Krane, S., Rodarte, J.C., Benbatoul, K.D., Dixon, R., Mjalli, A.M.M., 2000. 2,4,5-Trisubstituted imidazoles: novel nontoxic modulators of P-glycoprotein mediated multidrug resistance. Part 2. Bioorg. Med. Chem. Lett. 10, 2599–2601.

Sheldon, R.A., Downing, R.S., 1999. Heterogeneous catalytic transformations for environmentally friendly production. Appl. Catal. A: Gen. 189, 163–183.

Shylesh, S., Schünemann, V., Thiel, W.R., 2010. Magnetically separable nanocatalysts: bridges between homogeneous and heterogeneous catalysis. Angew. Chem. Int. Ed. 49, 3428–3459.

Sun, Y., Ma, M., Zhang, Y., Gu, N., 2004a. Synthesis of nanometer-size maghemite particles from magnetite. Colloids Surf. A 245, 15–19.

Sun, Y., Ma, M., Zhang, Y., Gu, N., 2004b. Synthesis of nanometer-size maghemite particles from magnetite. Colloid Surf. A 245, 15–19.

Sunita, G., Devassy, B.M., Vinu, A., Sawant, D.P., Balasubramanian, V.V., Halligudi, S.B., 2008. Synthesis of biodiesel over zirconia-supported isopoly and heteropoly tungstate catalysts. Catal. Commun. 9, 696–702.

Teimouri, A., Chermahini, A.N., 2011. An efficient and one-pot synthesis of 2,4,5-trisubstituted and 1,2,4,5-tetrasubstituted imidazoles catalyzed via solid acid nano-catalyst. J. Mol. Catal. A: Chem. 346, 39–45.

Thomas, J.M., 1992. Solid acid catalysts. Sci. Am. 266, 112–118.

Wang, L.-M., Wang, Y.-H., Tian, H., Yao, Y.-F., Shao, J.-H., Liu, B., 2006. Ytterbium triflate as an efficient catalyst for one-pot synthesis of substituted imidazoles through three-component condensation of benzil, aldehydes and ammonium acetate. J. Fluorine Chem. 127, 1570–1573.

Wang, L., Woods, K.W., Li, Q., Barr, K.J., McCroskey, R.W., Hannick, S.M., Gherke, L., Credo, R.B., Hui, Y.H., Marsh, K., Warner, R., Lee, J.Y., Zielinski-Mozng, N., Frost, D., Rosenberg, S.H., Sham, H.L., 2002. Potent, orally active heterocycle-based combretastatin A-4 analogues: synthesis, structure–activity relationship, pharmacokinetics, and in vivo antitumor activity evaluation. J. Med. Chem. 45, 1697–1711.

Wang, P., Kong, A.G., Wang, W.J., Zhu, H.Y., Shan, Y.K., 2010. Facile preparation of ionic liquid functionalized magnetic nanosolid acid catalysts for acetalization reaction. Catal. Lett. 135, 159–164.

Wang, X.C., Gong, H.P., Quan, Z.J., Li, L., Ye, H.L., 2009. PEG-400 as an efficient reaction medium for the synthesis of 2,4,5-triaryl-1*H*-imidazoles and 1,2,4,5-tetraaryl-1H-imidazoles. Chin. Chem. Lett. 20, 44–47.

Wu, L., Li, B.L., Huang, Y.Y., Zhou, H.F., He, Y.M., Fan, Q.H., 2006. Phosphine dendrimer-stabilized palladium nanoparticles, a highly active and recyclable catalyst for the Suzuki-Miyaura reaction and hydrogenation. Org. Lett. 8, 3605–3608.

Xuan, S., Jiang, W., Gong, X., Hu, Y., Chen, Z., 2008. Magnetically separable Fe_3O_4/TiO_2 hollow spheres: fabrication and photocatalytic activity. J. Phys. Chem. C 113, 553–558.

Zang, H., Su, Q., Mo, Y., Cheng, B.-W., Jun, S., 2010. Ionic liquid [EMIM]OAc under ultrasonic irradiation towards the first synthesis of trisubstituted imidazoles. Ultrason. Sonochem. 17, 749–751.

Zhao, Y., Tao, C., Xiao, G., Wei, G., Li, L., Liu, C., Su, H., 2016. Controlled synthesis and photocatalysis of sea urchin-like Fe_3O_4@TiO_2@Ag nanocomposites. Nanoscale 8, 5313–5326.